Journal of Sound and Vibration 329 (2010) 4367–4379

Contents lists available at ScienceDirect

Journal of Sound and Vibration

journal homepage: www.elsevier.com/locate/jsvi

Optimisation of axially segmented liners for aeroengine broadband noise

T.R. Law [a,*], A.P. Dowling [b], R. Corral [a]

[a] School of Aeronautics, Universidad Politécnica de Madrid, 28040 Madrid, Spain
[b] Engineering Department, University of Cambridge, Trumpington Street, Cambridge CB2 1PZ, UK

ARTICLE INFO

Article history:
Received 22 February 2010
Accepted 25 April 2010
Handling Editor: R.J. Astley
Available online 26 May 2010

ABSTRACT

A practical two-stage method for optimising an acoustic liner divided into axial segments for aeroengine broadband noise is presented. The principles are explained based on a three segment design but extension to more segments is straightforward. Initially, the optimisation focuses on the material properties of the individual segments. The second stage determines the optimum axial segment lengths and the optimum permutation of segments along the duct by evaluating the fully scattered acoustic field. This method is deployed to optimise an absorber for a broadband source noise of bandwidth 900 Hz–1.8 kHz. The axial order of the segments is found to have a dramatic influence on the optimum axial segment lengths. In the case study, comparisons with optimised uniform liners over this frequency range demonstrate only a small noise reduction. A simple optimisation that neglects scattering between axial segments significantly overestimates the available attenuation and provides a poor estimate of the optimum segment lengths.

1. Introduction

The continuous exponential growth of the air transport industry has led to sustained pressure on aeroengine manufacturers to reduce propulsion noise. The most apparent trend in civil turbofan engines has been the shift to larger bypass ratios primarily to reduce jet noise. Larger fan designs have focused more attention on blade noise with fan rearward broadband noise now emerging as one of the principal aircraft noise sources. A large proportion of the recent progress in noise suppression has been as a result of acoustic linings meaning the optimisation of the absorbers has become a critical part of the design process. In addition to the traditional porous facing sheet and resonant cavity acoustic liner, a number of other novel concepts have started to arise [1–10]. Perhaps the most fruitful of these is the 'zero splice' technology that will come into service in the near future [11]. The 'zero splice' refers to the absence of the periodic joints around the liner circumference that are usually present to facilitate manufacture and installation of the assembly. This technology is designed to avoid scattering between different azimuthal acoustic modes. In particular, to prevent scattering into lower azimuthal modes that are harder to absorb and therefore degrade the performance of the liner.

Elsewhere, it has been suggested that attenuation could be improved by increasing the scattering. The aptly named 'checkerboard' liner concept contains a large number of periodic discontinuities in both the radial and axial directions. Mani [12] and Howe [13] have suggested that a synergy of axial and radial discontinuities might be the best means of increasing attenuation. Clearly, one of the major challenges with such a system is the number of unknown variables. Aside

* Corresponding author.
E-mail address: tom.law@cantab.net (T.R. Law).

0022-460X/$ - see front matter Crown Copyright © 2010 Published by Elsevier Ltd. All rights reserved.
doi:10.1016/j.jsv.2010.04.029

from the impedance of the individual segments, one has also to consider the segment widths, lengths and the periodicity of the system. Watson et al. [10] have taken some initial design steps by deploying Finite Element methods in conjunction with a genetic optimisation algorithm on a rectangular sectioned duct. The results are encouraging and are due to be validated experimentally. However, as yet any application to aeroengine acoustic treatment is still a long way off.

As much of the focus has been on inlet noise where the length of the lined duct upstream of the fan is relatively short, less interest has been directed towards axial discontinuities. Lansing and Zorumski [14,15] were the first to publish research on this topic. Baumeister [16] and Tsai [17] reported that the first axial segment acts as a favourable scatterer for attenuation in later segments. However, the former suggested that significant advantages would only be available in low frequency single mode applications. More recently, McAlpine et al. [7] used a mode-matching technique based on the Galerkin method of weighted residuals [18]. An attenuation increase of 25 dB was predicted for the rotor-alone tone when using a two-segment inlet liner instead of a uniform one. Conventional fan designs contain a moderate number of blades leading to the associated tonal noise being represented as a small number of Tyler–Sofrin modes [19]. The forward-propagating rotor-alone pressure field that becomes cut-on at high power settings is frequently composed of a single disturbance of high azimuthal order. Axial scattering here will inevitably improve performance by transferring energy into higher cut-off radial modes.

The picture is less clear for multimode broadband sources. For these, scattering may transfer energy into both higher and lower order radial modes. In principle, one should be able to improve the attenuation bandwidth of the entire system by having a series of different axial segments 'tuned' to absorb a variety of frequencies. If the axial length and segment sequence is chosen carefully, there could be additional attenuation benefits from the scattering at segment interfaces. Law [20] has demonstrated that significant broadband noise benefits can exist for a concept aeroengine design with a large surface area available for lining. Conversely Lafronza et al. [21] have been unable to find much benefit when optimising a two segment inlet liner for broadband noise unless only a small number of modes are cut-on. In a contemporary setting, the complexities of the design and potential benefits are severely offset by the associated cost and manufacturing difficulties. In this paper, the authors wish to present a practical optimisation approach for such a system. A three segment liner will be designed to mitigate a broadband source. Optimisation will take place in two discrete stages. Firstly, individual segment material properties are considered in isolation. Axial segment lengths are then chosen whilst the segment sequence is also selected to maximise any benefits due to interface scattering. The final performance will then be compared with equivalent uniform absorbers and an approximation where the scattering at the segment interfaces is ignored.

2. Segmented liner model

2.1. Model development

A cylindrical system consisting of three axially spaced acoustic liner segments of total length L_T will be considered as shown in Fig. 1. At either end, lengths L_1 and L_5 of unlined or 'rigid' duct have been included to facilitate the analysis. This effectively increases the number of segments to five. In each segment, the flow is assumed to be inviscid and may be decomposed into a uniform mean flow with axial mean flow, M_x, and a small perturbation harmonic in time. The external wall is of radius a and the dth segment begins at axial position $x=x_0^d$. The specific acoustic impedances, Z_A, Z_B and Z_C, have been identified using letter subscripts to emphasise that the sequence of liner segments will be modified. Hence, the impedances do not correspond to the lined segment lengths L_2, L_3 and L_4. The acoustic pressure field in segment d referred to here as p^d satisfies the convected wave equation

$$\nabla^2 p^d = \frac{1}{c^2}\left[\frac{\partial}{\partial t} + cM_x\frac{\partial}{\partial x}\right]^2 p^d. \tag{1}$$

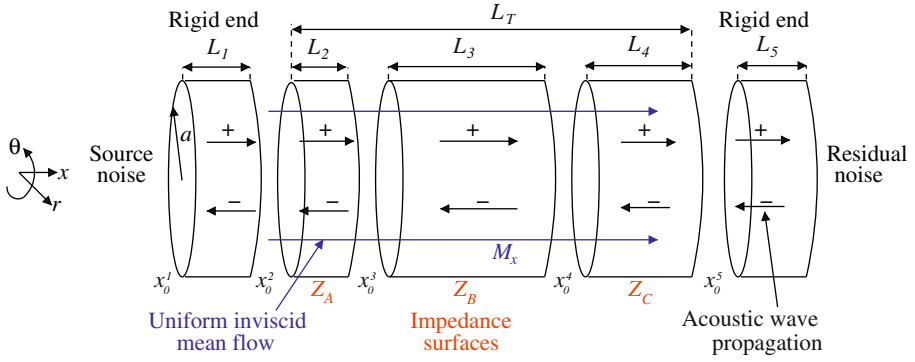

Fig. 1. Segmented liner optimisation model.

The familiar solution in a cylindrical coordinate system (r,θ,x) where $p^d=\hat{p}^d\exp(i\omega t)$ consists of a modal expansion of upstream $(-)$ and downstream $(+)$ travelling disturbances that is convenient to express as

$$\hat{p}^d(r,\theta,x)=\sum_{m=-\infty}^{\infty}\sum_{n=1}^{\infty}\hat{p}_{nm}^{d+}+\hat{p}_{nm}^{d-}=\sum_{m=-\infty}^{\infty}\sum_{n=1}^{\infty}e^{-im\theta}[A_{mn}^{d+}\exp(-ik_{x,mn}^{d+}(x-x_0^d))J_m(k_{r,mn}^{d+}r)+A_{mn}^{d-}\exp(-ik_{x,mn}^{d-}(x-x_0^{d+1}))J_m(k_{r,mn}^{d-}r)]. \tag{2}$$

Here, m and n are the azimuthal and radial modes, k_x and k_r are wavenumbers in the axial and radial directions and J_m denotes the m th-order Bessel function of the first kind. For example, $k_{x,mn}^{d-}$ represents the upstream propagating axial wavenumber for mode (m,n) in segment d. Complex modal amplitude coefficients are set at either the upstream end of a segment for downstream propagating modes or the downstream end for upstream propagating modes. That is A_{mn}^{d+} are defined at axial position $x=x_0^d$ and A_{mn}^{d-} are defined at $x=x_0^{d+1}$. The reason for this additional layer of complexity will become apparent later when discussing the mode matching formulation. In a uniform axial mean flow, Eq. (2) satisfies the convected wave equation if the axial and radial wavenumbers are related to the free space wavenumber, $k=\omega/c$, by the dispersion relationship

$$k_{x,mn}^{d\pm}=\frac{-kM_x\pm\sqrt{k^2-(1-M_x^2)(k_{r,mn}^{d\pm})^2}}{1-M_x^2}. \tag{3}$$

In a rigid walled duct, the boundary condition at either wall is zero radial pressure gradient. The radial wavenumbers will then satisfy $J_m'(k_{r,mn}a)=0$. The prime denotes differentiation with respect to the argument and the solutions are readily available. The $\pm$ superscripts have been dropped to recognise that an upstream propagating mode will have the same radial wavenumber as the downstream one under rigid wall conditions. This set of solutions for $k_{r,mn}$ are denoted κ_{mn}. At a fixed frequency, in a rigid walled duct, only a finite number of modes can propagate inside the duct and transmit acoustic power. All other modes are referred to as cut-off and transmit no acoustic power. The cut-off ratio, ζ_{mn} is defined as

$$\zeta_{mn}=\frac{k}{\kappa_{mn}\sqrt{1-M_x^2}}. \tag{4}$$

Under these conditions, Eq. (3) may be rewritten in terms of ζ_{mn} as

$$k_{x,mn}^{d\pm}=\frac{-kM_x\pm k\sqrt{1-(1/\zeta_{mn})^2}}{1-M_x^2}. \tag{5}$$

Hence ζ_{mn} controls the sign of the square root. Mode (m,n) propagates inside the duct or is cut-on if $\zeta_{mn}>1$, otherwise it is cut-off and physically acceptable solutions indicate modes that decay exponentially along the duct. For each azimuthal mode order m, the radial modes are ordered in terms of decreasing cut-off ratio, i.e. $\zeta_{m1}>\zeta_{m2}>\zeta_{m3}\ldots$. This is equivalent to ordering in terms of increasing κ_{mn}. Radial modes $n>n_{m,c}$ are cut-off, the m subscript indicates that this is a function of azimuthal mode number. For a particular value of m, the number of cut-on radial modes rapidly decreases as $|m|\to\infty$. Therefore, azimuthal orders $|m|>m_c$ contain no propagating radial modes and are also cut-off. The correct linearised boundary condition for a general locally reacting geometry assuming an infinitely thin vortex sheet was derived by Myers [22]. In the case of a straight axisymmetric duct with a uniform axial inviscid flow, this expression reduces to continuity of particle displacement at the duct wall where $r=a$. This condition is defined by Eq. (6) where the segment superscripts d have been temporarily omitted to improve clarity

$$\frac{\partial\hat{p}_{mn}^{\pm}}{\partial r}=-\frac{ik}{Z}\left[1-\frac{M_xk_{x,mn}^{\pm}}{k}\right]^2\hat{p}_{mn}^{\pm}. \tag{6}$$

The normalised acoustic wall impedance is represented by Z. From Eq. (6), the eigenvalue equation can be derived by inserting the expression for acoustic pressure from Eq. (2)

$$[mZ+ika(1-M_xk_{x,mn}^{\pm}/k)^2]J_m(k_{r,mn}^{\pm}a)-k_{r,mn}^{\pm}aZJ_{m+1}(k_{r,mn}^{\pm}a)=0. \tag{7}$$

As the non-rigid or lined radial wavenumbers that are sought tend to remain close to the real axis, these modes will be ordered based on the equivalent rigid wall wavenumbers. The solutions to Eq. (7) can be obtained using Newton–Raphson iteration departing from the rigid wall solutions using a continuation method where the continuation parameter is the impedance. The method is similar to one described by Eversman [23] and more details can be found in Ref. [20] if desired.

The eigenvalue problem is solved in non-dimensional form where the duct radius, a, and sound speed, c, are used to normalise the input variables. In the case study that will be investigated in due course, a = 0.60 m and c = 364 ms^{-1}, the flow has an axial Mach number of 0.47 and a total lined duct length, L_T, of two duct diameters, 2D or 4a. The values are representative of those that could be present in the exhaust flow of a contemporary turbofan engine during take-off. Determination of suitable impedance values will be considered in Section 3.

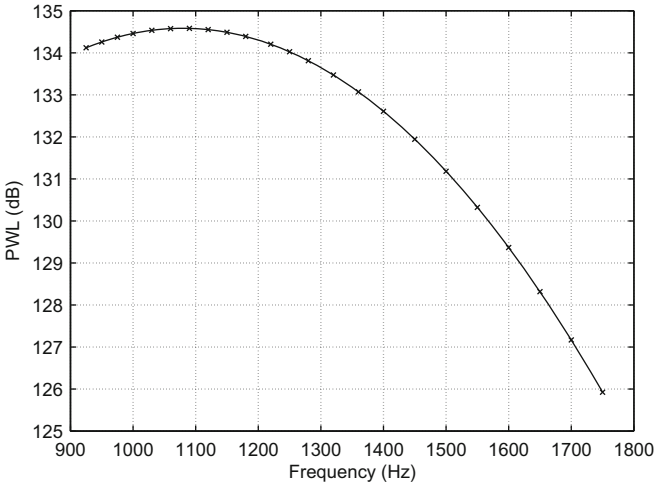

Fig. 2. Input broadband PWL spectrum, ref. 1×10^{-12} W.

2.2. Source noise definition

A broadband noise spectrum across a frequency band that ranges from 0.9 to 1.8 kHz will be considered. The spectrum will be modelled as a series of multimode calculations at the twenty three 1/24th octave centre frequencies that exist between the limits specified. The acoustic power level (PWL) spectrum against which to optimise the liner design is shown in Fig. 2. The spectrum is representative of that produced by the fan during take-off. All PWL values are referenced to 1×10^{-12} W.

The acoustic power associated with any particular mode is given by integrating the axial intensity or acoustic power per unit area, $I_x^{\pm}$, over the duct cross-sectional area

$$W_{mn}^{\pm}=2\pi\int_0^a I_{x,mn}^{\pm} r\,\mathrm{d}r. \tag{8}$$

An expression for the modal acoustic intensity in the presence of a mean flow has been given by Morfey as Eq. (16) in Ref. [24]. This can be expressed as

$$I_{x,mn}^{\pm}=\frac{|p_{mn}^{\pm}|^2}{2\rho c}[(1+M_x^2)\mathrm{Re}\{\eta_{mn}^{\pm}\}+M_x(1+|\eta_{mn}^{\pm}|^2)], \tag{9}$$

$$\eta_{mn}^{\pm}=\frac{k_{x,mn}^{\pm}a}{ka-M_x k_{x,mn}^{\pm}a}. \tag{10}$$

In the case of the rigid wall, the orthogonality of the mode shapes allows individual modal powers to be added directly to determine overall power. This dramatically simplifies the allocation of incident modal amplitudes. The following result is obtained by evaluating Eq. (8) analytically

$$W_{mn}^{\pm}=\frac{\pi a^2}{2\rho c}|A_{mn}^{\pm}|^2[(1+M_x^2)\mathrm{Re}\{\eta_{mn}^{\pm}\}+M_x(1+|\eta_{mn}^{\pm}|^2)]\left[1-\left(\frac{m}{\kappa_{mn}a}\right)^2\right]|J_m(\kappa_{mn}a)|^2. \tag{11}$$

This will also become useful for allocating appropriate modal amplitudes. In this investigation, the commonly made assumption of equal power per incident cut-on mode will be made to model all broadband sources. In addition, all modes will be initialised with equal phase. Lafronza et al. [21] have demonstrated that the phasing between modes has only a small effect on the transmitted power for multimode calculations such as this.

Later, it will become instructive to consider the transfer of acoustic energy between modes as the disturbances propagate downstream. As the propagation is through a series of lined walls, the radial modes are no longer orthogonal. This means that the analytical solution of Eq. (11) is not valid and modal powers cannot be summed within lined ducts. The evaluation of acoustic intensity for multiple modes now contains a series of cross-terms that may be of significant magnitude depending on the phasing of the modes. At this point, the contributions of individual modes to the overall energy flow rate becomes ambiguous. The approach taken here is to split the contribution from a cross-term equally between the two modes involved. This leads to an expression for the modal intensity, which ensures that the summation over N_m radial mode energies gives the correct total power. If one observes that the modal axial velocity $u_{x,mn}^{\pm}=\eta_{mn}^{\pm}p_{mn}^{\pm}$

then the modal intensity can be rewritten as Eq. (12) where * denotes the complex conjugate

$$I_{mn}^{\pm}=\frac{1}{4\rho c}\mathrm{Re}\left\{\sum_{i=1}^{N_m}(1+M_x^2)[(p_{mn}^{\pm})^*u_{x,mi}^{\pm}+(p_{mi}^{\pm})^*u_{x,mn}^{\pm}]+M_x[(p_{mn}^{\pm})^*p_{mi}^{\pm}+(p_{mi}^{\pm})^*p_{mn}^{\pm}+(u_{x,mn}^{\pm})^*u_{x,mi}^{\pm}+(u_{x,mi}^{\pm})^*u_{x,mn}^{\pm}]\right\}. \quad (12)$$

This expression will be revisited in Section 5.2.

3. Segment optimisation

The first stage in the optimisation is to choose the material properties of the three segments. For a single layer liner (see Fig. 3), there are a number of material parameters to vary. The most influential ones are the facing sheet porosity (porosity defined as the fractional surface area occupied by the holes) and the backing cell depth. Others such as facing sheet thickness and perforate hole diameter will typically improve by being reduced and are therefore set by material and manufacturing restrictions rather than performance estimates. As a result, all other values have been set to existing industry designs (thickness: 0.56 mm, hole diameter: 1.40 mm) and only changes in the main two are considered. To compute the eigenvalues in Eq. (7), values of Z are required rather than material properties. This necessitates a liner impedance model. The finer details of the liner impedance model used are not central to this paper and as such are not given here. The interested reader is directed towards Refs. [20,25,26] for suitable techniques to extract impedance values from liner dimensions. The impedance values extracted from the model are semi-empirical and are primarily a function of frequency, axial Mach number, facing sheet thickness, porosity, perforate hole diameter and backing cell depth. The liner backing depth has the strongest influence on setting the frequency of peak attenuation (and liner reactance). Using simple standing wave principles, one would expect optimum cell depth to be close to a quarter of the wavelength of the incident sound.

The liner resistance is largely dictated by the facing sheet porosity and crucially is independent of the cell depth. Hence, a cell depth may be chosen and the porosity adjusted to maximise performance at the peak attenuation frequency. For this investigation, a final design is sought that will provide good attenuation across the whole band 0.9–1.8 kHz. Therefore,

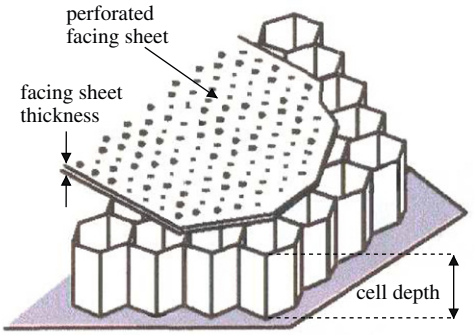

Fig. 3. Conventional single layer liner design.

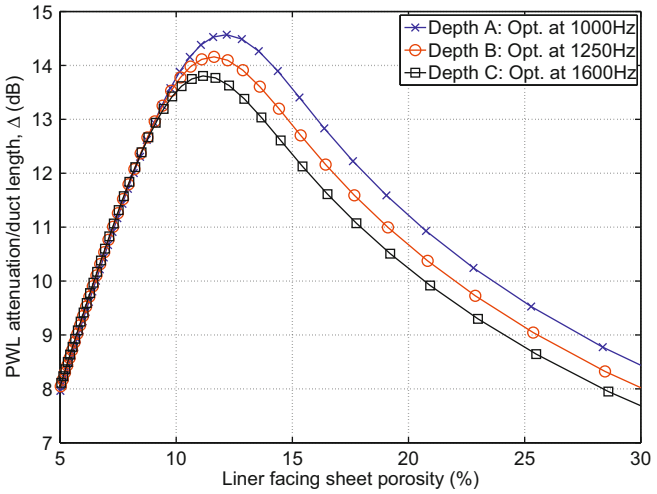

Fig. 4. Variation in PWL attenuation with facing sheet porosity for the chosen three liner backing depths at their design frequencies.

backing depths are chosen to provide good attenuation at the three third octave centre frequencies, 1, 1.25 and 1.6 kHz. These are 84.4, 66.1 and 50.2 mm, respectively. For an absorber with axial length equal to the duct diameter, D, PWL attenuation assuming equal incident power per mode can be estimated using Eq. (13) where the summation is over all cut-on modes

$$\Delta = \frac{\sum_{m=-m_c}^{m_c} n_{m,c}}{\sum_{m=-m_c}^{m_c} \sum_{n=1}^{n_{m,c}} \exp(2\,\mathrm{Im}(k_{x,mn}^{+} D))}. \tag{13}$$

This can be used as a metric for choosing an appropriate facing sheet porosity. If Eq. (13) is evaluated at the chosen backing depths for the specified duct conditions, the variation with facing sheet porosity in Fig. 4 can be obtained. A simple routine can then be executed to determine the optimum values. The corresponding porosity values obtained from the impedance model are 12.06 percent (84.4 mm), 11.60 percent (66.1 mm) and 11.22 percent (50.2 mm). These segment designs will be referred to as A, B and C from now on. The porosity values compare well with porosities of liners currently in service. Using these parameters, impedance values for each segment at each frequency have been computed and are plotted in the Appendix to this paper.

4. Axial length optimisation

4.1. Mode matching formulation

Unlike individual segment optimisation, choosing the axial lengths of each segment has to account for the incident pressure field and the effects of acoustic scattering at each segment interface. Forming a metric requires a means of estimating the attenuation provided by the sequence of three segments (plus rigid ends) axially spaced along a duct. The chosen approach is based on the work of McAlpine et al. [7]. At each interface, the aim is to match the acoustic pressure and axial velocity, u_x, across the entire cross-section using the method of weighted residuals [18].

As the system has rotational symmetry, there is no scattering between azimuthal modes and therefore each azimuthal mode can be considered separately. If the harmonic pressure field for azimuthal mode m is truncated to a suitable number of radial modes, N_m, it can be expressed as

$$\hat{p}_m^d(r,\theta,x) = \mathrm{e}^{-\mathrm{i}m\theta} \sum_{n=1}^{N_m} [A_{mn}^{d+} \exp(-\mathrm{i}k_{x,mn}^{d+}(x-x_0^d)) J_m(k_{r,mn}^{d+} r) + A_{mn}^{d-} \exp(-\mathrm{i}k_{x,mn}^{d-}(x-x_0^{d+1})) J_m(k_{r,mn}^{d-} r)]. \tag{14}$$

The two sets of N_m equations to be solved at a liner interface, d, are given by

$$\int_0^a r J_m(\kappa_{mn} r)[\hat{p}_m^{d+1}(r,\theta,x_d^+) - \hat{p}_m^d(r,\theta,x_d^-)]\,\mathrm{d}r = 0, \tag{15}$$

$$\int_0^a r J_m(\kappa_{mn} r)[\hat{u}_{x,m}^{d+1}(r,\theta,x_d^+) - \hat{u}_{x,m}^d(r,\theta,x_d^-)]\,\mathrm{d}r = 0. \tag{16}$$

The weighting terms at the front of the integration $rJ_m(\kappa_{mn} r)$ are the rigid wall eigenfunctions. These terms are included so that the integral can be evaluated analytically speeding up the solution time. In addition, orthogonality can be exploited in any rigid wall sections. The plus and minus sign superscripts on x_d indicate that the pressure and velocity solutions in the dth duct are being matched immediately downstream and upstream of the liner junction.

The relationship between acoustic pressure and axial velocity is derived from the acoustic axial momentum equation where $\eta_{nm}^{\pm}$ was defined in Eq. (10)

$$\hat{u}_{x,mn}^{\pm} = \frac{\eta_{mn}^{\pm} \hat{p}_{mn}^{\pm}}{\rho c}. \tag{17}$$

4.2. Mode matching matrices

The solution method involves the creation of four transfer matrices, one for each interface. It is convenient to express the match at the dth interface between segment d and $d+1$ for the chosen azimuthal order as the matrix equation

$$\begin{bmatrix} A_m^{(d+1)+} \\ \cdots\cdots\cdots \\ A_m^{d-} \end{bmatrix} = \mathbf{T}^d \mathbf{D}^d \begin{bmatrix} A_m^{d+} \\ \cdots\cdots\cdots \\ A_m^{(d+1)-} \end{bmatrix}. \tag{18}$$

Modes on the left hand side are travelling away from the interface and modes on the right hand side are travelling towards the interface. Eq. (18) consists of a $2N_m \times 2N_m$ transfer matrix, $\mathbf{T}^d$, and corresponding decay matrix, $\mathbf{D}^d$, a diagonal matrix of the same size. The definition of the modal amplitudes, $A_{mn}^{d\pm}$, at the segment interface locations rather than

the origin has greatly simplified the formulation here. The amplitude matrices, A_m^d, consist of an $N_m \times 1$ vector with the nth entry corresponding to radial mode n. The decay matrices describe the decay over the length of the segment and so convert the amplitudes at one end of the segment to those at the other. The matrix entries are defined here for each segment

$$\mathbf{T}^d = \left[\begin{array}{c|c} \alpha^{(d+1)+} & -\alpha^{d-} \\ \cdots\cdots\cdots\cdots & \\ \beta^{(d+1)+} & -\beta^{d-} \end{array}\right]^{-1} \left[\begin{array}{c|c} \alpha^{d+} & -\alpha^{(d+1)-} \\ \cdots\cdots\cdots\cdots & \\ \beta^{d+} & -\beta^{(d+1)-} \end{array}\right]. \tag{19}$$

Each matrix quadrant represents a square matrix, size $N_m \times N_m$. Each element (i,j) of $\alpha^{d\pm}$ and $\beta^{d\pm}$ is defined below. As before, κ_{mn} denotes the value of the radial wavenumber $k_{r,mn}^{d\pm}$ under rigid wall conditions

$$\alpha_{ij}^{d\pm} = \int_0^a r J_m(\kappa_{mi} r) J_m(k_{r,mj}^{d\pm} r)\,\mathrm{d}r, \tag{20}$$

$$\beta_{ij}^{d\pm} = \frac{k_{x,mj}^{d\pm}\alpha_{d,ij}^{\pm}}{k - M_x k_{x,mj}^{d\pm}}. \tag{21}$$

The integral in Eq. (20) can be evaluated analytically

$$\alpha_{ij}^{d\pm} = \frac{a}{\kappa_{mi}^2 - (k_{r,mj}^{d\pm})^2}\{\kappa_{mi} J_{m+1}(\kappa_{mi} a) J_m(k_{r,mj}^{d\pm} a) - k_{r,mj}^{d\pm} J_m(\kappa_{mi} a) J_{m+1}(k_{r,mj}^{d\pm} a)\}. \tag{22}$$

For the rigid sections, the computation can take advantage of the orthogonality relationship of the Bessel functions for further simplification

$$\alpha_{ij}^{d\pm} = \begin{cases} \dfrac{a^2}{2}\left[1 - \left(\dfrac{m}{\kappa_{mi} a}\right)^2\right] J_{mi}^2(\kappa_{mi} a) & \text{if } i = j, \\ 0 & \text{if } i \neq j. \end{cases} \tag{23}$$

In the plane wave case, $\kappa_{mn} = 0$ and the limiting value of Eq. (23) when $i=j$ becomes $\frac{1}{2}a^2$. The non-zero entries of the diagonal matrix $\mathbf{D}^d$ are defined as Eq. (24) where L_d is the axial length of the dth segment

$$\mathbf{D}_{ii}^d = \begin{cases} \exp[-\mathrm{i} L_d k_{x,mi}^{d+}], & i = 1,2,\ldots,N_m, \\ \exp[-\mathrm{i} L_{d+1} k_{x,mi}^{(d+1)-}], & i = N_m+1,\ldots,2N_m. \end{cases} \tag{24}$$

4.3. Computation and boundary conditions

The boundary condition at the inlet is the input noise field defined in Section 2.2. To simplify matters, the boundary condition at the downstream end of the duct is assumed to be anechoic. It would be straightforward to incorporate a reflection coefficient into the model if desired.

The specification of upstream and downstream boundary conditions together with Eqs. (15) and (16) leads to $8N_m$ equations and the same number of unknown coefficients. Hence, at frequencies with a large number of radial modes, the matrix equations can become very large and a direct matrix solver is likely to be very time-consuming. A more intelligent solution scheme involves an iterative marching procedure proposed by Cummings [27]. In general, the eigenvalues in each liner segment will not vary drastically from the rigid wall values and consequently from one other. As a result, all amplitudes are initialised to zero except A_{mn}^{1+} (a reflective downstream boundary condition would also result in A_{mn}^{5-} being non-zero). Eq. (18) is evaluated once to obtain estimates for the values on the left hand side at each interface in turn. Updated values are inserted into subsequent interface calculations as they become available. Once there is no appreciable change in all amplitudes, the system has converged. This will typically require one second of CPU time per azimuthal order on a standard desktop PC. Convergence for the matches between rigid end sections and adjacent segments is slightly more difficult to achieve. This is due to the radial eigenvalues on one side of the match having no imaginary component. A quick and simple remedy is to add a small imaginary part and converge to an intermediate solution. This can then be used to re-converge to the desired solution. The entire scheme has been found to be incredibly robust for realistic liner parameters and during extensive testing has not been known to fail.

4.4. Radial mode truncation error

Clearly, since there is an infinite number of radial modes for each value of m, it becomes necessary to truncate the number appropriately to derive an acceptable solution. McAlpine et al. [7] have suggested that if there are less than five

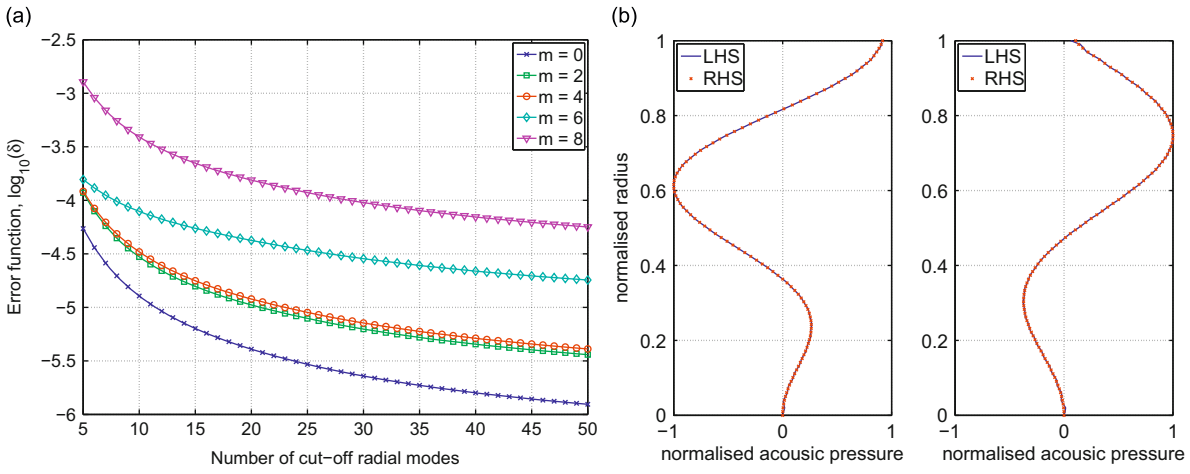

Fig. 5. Mode matching example at 1 kHz for segment order A B C, segment lengths $[L_2\ L_3\ L_4] = [0.75D\ 0.00\ 1.25D]$ at the first interface, $x = x_0^2$. (a) Variation of $\log_{10}(\delta_m^d)$ with radial mode truncation length. (b) Pressure match, $m = 2$, 30 cut-off radial modes.

radial modes cut-on, a total of 20 radial modes appears sufficient. The highest frequency considered here results in the propagation of up to seven radial modes (this is for $m = 0$ at 1750 Hz). Thus to ensure that the results are reliable, 30 additional cut-off modes have been included for each calculation performed irrespective of the frequency. An estimate of the quality of the match can be determined by evaluating a mean squared error function, δ_m^d, defined in

$$\delta_m^d = \frac{\int_0^a |\hat{p}_m^{d+1}(r,\theta,x_d^+) - \hat{p}_m^d(r,\theta,x_d^-)|^2\,\mathrm{d}r}{\int_0^a |\hat{p}_m^{d+1}(r,\theta,x_d^+)|^2\,\mathrm{d}r}. \tag{25}$$

Fig. 5 shows how the accuracy improves at $x = x_0^2$ when more cut-off modes are included for a selection of azimuthal mode numbers at 1 kHz using the original segment sequence. A pressure match corresponding to $m = 2$ with 30 cut-off modes is also displayed.

4.5. Comparison with no scatter prediction

The mode matching formulation above provides a relatively quick way of computing the fully scattered acoustic field. It is possible to compute an approximation by neglecting the interface scattering between segments. This is achieved by assuming that there is no reflection and that the squared amplitude of the downstream propagating modes is only modified by the modal decay rate in each segment. Thus, the modal power is reduced in each segment by a factor of $\exp[2\,\mathrm{Im}(k_{x,mn}^{q+}L_q)]$ and the squared amplitude that reaches the downstream rigid segment can be estimated using

$$|A_{mn}^{5+}|^2 = |A_{mn}^{1+}|^2 \prod_{q=2}^{4} \exp[2\,\mathrm{Im}(k_{x,mn}^{q+}L_q)]. \tag{26}$$

This is in line with methods used elsewhere [28,29]. The total residual power in a rigid duct is then computed in the familiar way using Eq. (11) and summing the modal contributions. Clearly, using a model such as this means that the segment order becomes unimportant as the only effect of the segment ordering is to change the scattering at each axial interface.

5. Segment length optimisation

5.1. Results

The impedances of the three liner segments have already been defined, which in turn fixes the eigenvalues. In fact, the only remaining independent parameters are the axial lengths, L_2, L_3 and L_4 of the segments. Given that the total duct length has also been fixed, this number is further reduced to two. Hence, for a given sequence of segments, a simple optimisation routine can be executed to determine the lengths that minimise the overall residual power level integrated over the entire frequency band. This requires approximately 30 minutes of processing time on a desktop PC using the matlab optimisation gradient method `fmincon`. There is no immediately obvious way to optimise the sequence, so all six segment permutations will be evaluated separately. The results are summarised in Table 1 and the match error function δ_m^d was monitored throughout. The same optimisation framework was used to compute the no scatter result, however the

Table 1
Optimum lengths for each segment order and corresponding metric.

Sequence	Optimum segment length–diameter ratio			Metric value (dB)
	A	B	C	
A B C	0.7519	0.0000	1.2481	130.71
A C B	0.7437	0.0882	1.1680	130.69
B A C	0.4766	0.2618	1.2616	130.49
B C A	0.0000	0.8825	1.1175	131.01
C A B	0.3011	1.4475	0.2514	130.94
C B A	0.0000	1.7813	0.2187	131.15
No scatter	0.1165	0.7094	1.1741	126.90

Table 2
Uniform liner comparison.

Uniform liner	Metric value (dB)
A	132.70
B	131.37
C	131.53

computation time required for this is of the order of one minute and there is no need to evaluate the six different segment permutations (Table 2).

In order to ensure that the true optimum has been found for each set of segment orders, six contour plots of residual PWL have been constructed (Fig. 6). To facilitate comparison between plots, the length–diameter ratios of segments A and B have been maintained as the vertical and horizontal axes, respectively, as have the contour limits for the metric. The values in the corners correspond to the results for uniform liners, i.e. the top left corner is a uniform segment A liner, bottom right hand corner is a uniform segment B liner and the origin is a uniform segment C liner.

The immediate observation is that the variation across all results is relatively small, 2.2 dB between the best and the worst system. The position of the optimum changes substantially across the six contour plots, which suggests that the permutation of the segments is a significant variable when attempting this type of calculation. If the segment lengths are adjusted to the optimum ones for each permutation, the variation in the metric across all six can be reduced to 0.66 dB. The overall optimum design occurs for segment sequence B A C where the value of the metric is 130.49 dB. For this system the performance across the whole frequency spectrum has been plotted in Fig. 7 alongside the performance of the three uniform liners. Clearly liner A alone is not well suited to the problem, however liner B can provide a large amount of the performance of the optimum design. The no scatter result provides an overestimate of the available attenuation from the three segments with rigid ends (3.59 dB compared to the optimum design). Therefore, at these frequencies, one may conclude that scattering has a detrimental effect on the acoustic performance. The optimum segment lengths also bear little resemblance to any of the other results.

5.2. Modal energy analysis

Further interrogation of the results shows that substantial performance improvements have not been achieved here because of the definition of the source noise. Even at the lowest frequency there are several radial modes cut-on. Thus scattering at each interface may transfer acoustic energy into both lower order and higher order radial modes. Unfortunately, it appears that scattering into lower order radial modes (that are normally less well attenuated by the liners) is at least as efficient if not more so than scattering into higher order radial modes. The comparison with the no scatter result (where the attenuation prediction increases if you ignore the scattering) also supports this observation. For example, consider Fig. 8. This shows the residual PWL in the downstream propagating radial modes upstream ($-$) and downstream ($+$) of each segment interface at 1.6 kHz for the optimum segmented liner. This was computed using Eq. (12) and the duct inlet and outlet are represented by 0 and 5, respectively. What one observes here is indicative of the general situation. There are instances when the scattering is beneficial (in this case, at interface 2) and energy is scattered into faster decaying modes. However, there are also instances where the opposite is true (in this case, interface 4). Hence, when there is energy in a large number of cut-on modes any beneficial effects due to scattering will most likely be cancelled out, especially over shorter distances.

These findings are consistent with those of Law [20] and Lafronza et al. [21] who have suggested that appreciable benefits for broadband noise are more likely to be achievable at lower frequencies where a segmented liner would also be able to outperform a no scatter prediction. For this reason, a uniform liner across this bandwidth can provide the majority of the performance benefits here. It seems performance could be improved relative to a uniform absorber if a wider

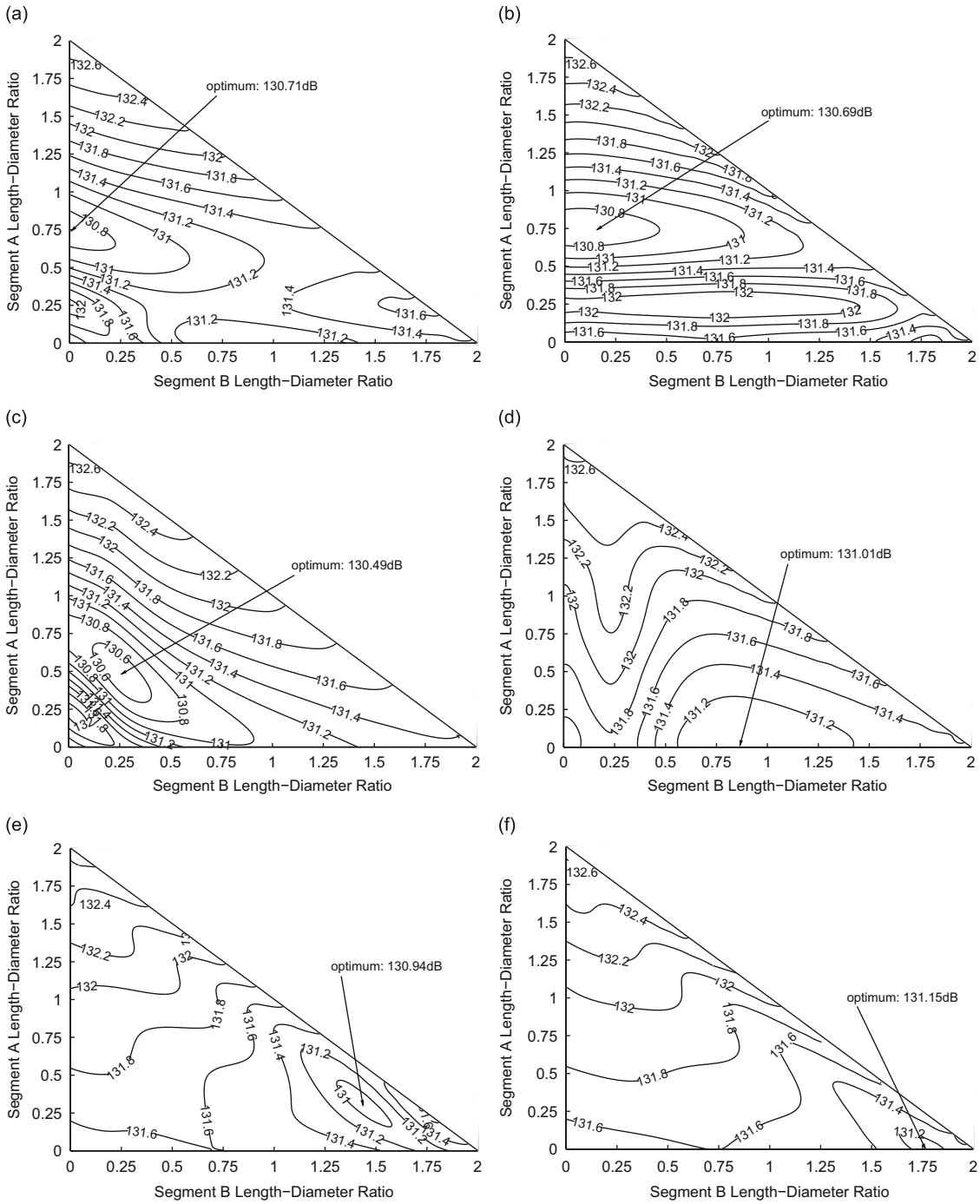

Fig. 6. Residual PWL contour plots showing optimum segment lengths for each segment order. (a) Segment order A B C. (b) Segment order A C B. (c) Segment order B A C. (d) Segment order B C A. (e) Segment order C A B. (f) Segment order C B A.

bandwidth was considered. The frequencies then become further away from the peak absorption frequency of the uniform absorber (the principal reason why liner A performs less well).

Finally, although overall attenuation has not been improved substantially, neither has it suffered from the additional scattering. One might dispute this with reference to the no scatter result, however this result is not achievable as the scattering from the rigid ends will always be present. Therefore, it is possible that broadband performance could be maintained whilst improving the attenuation of a tone where the majority of the acoustic energy was in the first radial mode. The inevitable scattering of the tone into higher order radial modes would then most likely improve overall liner performance.

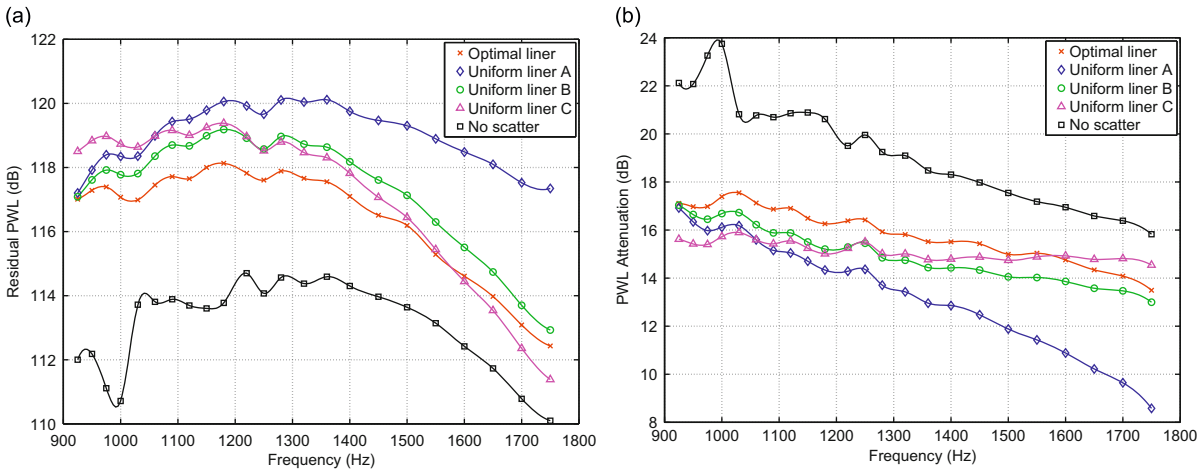

Fig. 7. Optimum design performance across the whole frequency band, comparison with uniform liners and no scatter prediction. (a) Residual PWL comparison. (b) PWL attenuation comparison.

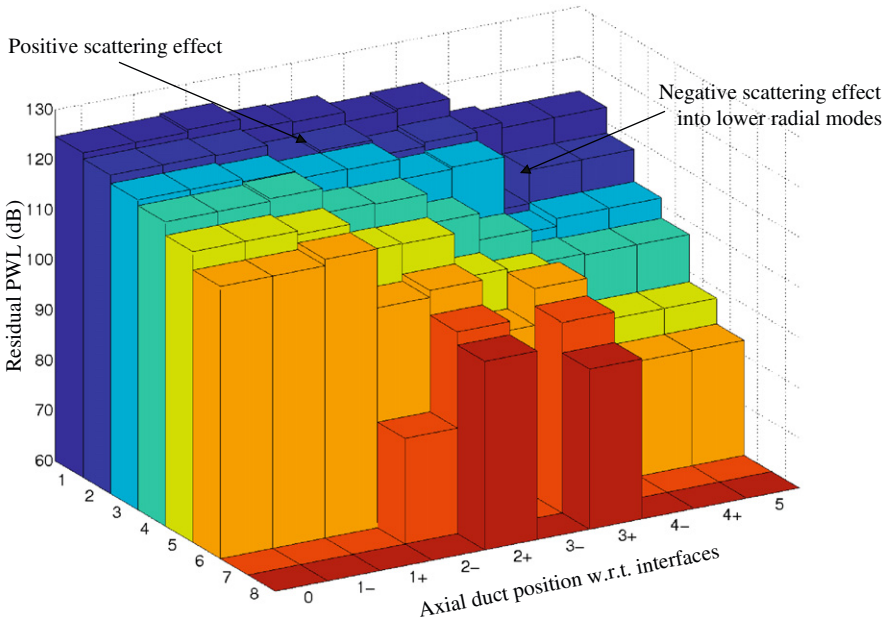

Fig. 8. Downstream propagating radial mode energy at segment interfaces for the optimum segmented liner at 1.6 kHz.

6. Conclusion

In this paper, a practical straightforward method to optimise an axially segmented liner for broadband noise attenuation has been presented. This has been used to investigate the potential benefits of such an absorber compared to a uniform liner. The design considered consisted of three segments and a broadband source spectrum between 900 Hz and 1.8 kHz. Acoustic mode matching at the segment interfaces was completed using the method of weighted residuals. The main observation was that the segmented design could only provide a small improvement over an optimised uniform liner (0.88 dB further reduction in acoustic power attenuation). During the investigation, the sequence of the liner segments was also varied. The segment sequence had a dramatic effect on the axial length of each segment required. Comparable overall performance could be achieved with each permutation but the axial lengths had to be substantially readjusted. Variation in optimum acoustic power attenuation across all sequences was then 0.66 dB.

It is suggested that to see higher performance benefits on broadband noise with an axially segmented liner, the acoustic energy should be concentrated in fewer radial modes. This would be the case at lower frequencies and then the energy scattered into higher radial modes would be more highly attenuated. This conclusion is supported by a crude optimisation

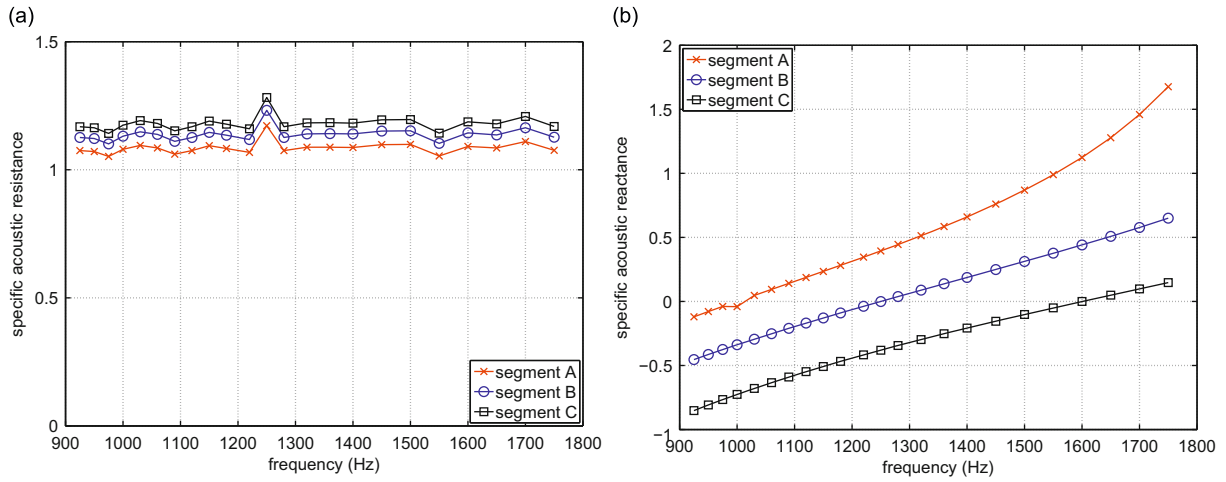

Fig. 9. Specific acoustic impedance values, Z, vs. frequency for each liner segment. (a) Specific acoustic resistance. (b) Specific acoustic reactance.

which ignores all scattering and subsequently overpredicts the available attenuation from the system. Furthermore, these results also demonstrate that the inter-segment scattering cannot be neglected for an accurate prediction of the optimum segment lengths and permutation. As broadband noise appears not to be adversely affected by the presence of scattering at segment interfaces, there is the potential for improving tonal attenuation with segmented liners whilst maintaining broadband performance. Finally, a design containing segments with greater impedance variations would increase interface scattering. Investigating such a system over a larger frequency bandwidth might also generate attenuation improvements.

Acknowledgements

The first author wishes to acknowledge the financial support received during his Ph.D. from the Engineering and Physical Sciences Research Council and the Cambridge-MIT Institute which was used to develop much of the software for this paper.

Appendix A. Liner segment impedance values

This appendix provides plots of the impedance values used for each of the three liner segments at each frequency (Fig. 9).

References

[1] J.S. Alonso, R.A. Burdisso, H.W. Kwan, S. Byrne, E. Chien, Experimental investigation of the HQ-liner concept on a scale simulated turbofan rig, *11th AIAA/CEAS Aeroacoustics Conference* (*26th AIAA Aeroacoustics Conference*), *AIAA*-2005-3070, Monterey, CA, 2005.
[2] P. Bartlett, N. Humphreys, P. Phillipson, J. Lan, E. Nesbitt, J. Premo, The Joint Rolls-Royce/Boeing Quiet Technology Demonstrator Programme, *10th AIAA/CEAS Aeroacoustics Conference* (*25th AIAA Aeroacoustics Conference*), *AIAA*-2004-2869, Manchester, UK, 2004.
[3] R.A. Burdisso, W. Ng, NASA CR-2003-212097: fan noise control using Herschel–Quincke resonators, Technical Report, 2003.
[4] D.H. de la Riva, R.A. Burdisso, W. Ng, Aft-fan noise control using Herschel/Quincke-liner systems, *11th AIAA/CEAS Aeroacoustics Conference* (*26th AIAA Aeroacoustics Conference*), *AIAA*-2005-3071, Monterey, CA, 2005.
[5] I.D.J. Dupere, A.P. Dowling, T. Lu, Optimization of cell structures of cellular materials for acoustic applications, *12th International Congress on Sound and Vibration*, Lisbon, Portugal, 2005.
[6] X. Jing, X. Wang, X. Sun, Broadband acoustic liner based on the mechanism of multiple cavity resonance, *13th AIAA/CEAS Aeroacoustics Conference* (*28th AIAA Aeroacoustics Conference*), *AIAA*-2007-3537, Rome, Italy, 2007.
[7] A. McAlpine, R.J. Astley, V.J.T. Hii, N.J. Baker, A.J. Kempton, Acoustic scattering by an axial-segmented turbofan inlet duct liner at supersonic fanspeeds, *Journal of Sound and Vibration* 294 (2006) 780–806.
[8] A. McAlpine, M.C.M. Wright, Acoustic scattering by a spliced turbofan inlet duct liner at supersonic fan speeds, *Journal of Sound and Vibration* 292 (2006) 911–934.
[9] C.K.W. Tam, H. Ju, Scattering of acoustic duct modes by axial liner splices, *12th AIAA/CEAS Aeroacoustics Conference* (*27th AIAA Aeroacoustics Conference*), *AIAA*-2006-2459, Cambridge, MA, 2006.
[10] W.R. Watson, J.H. Robinson, M.G. Jones, T.L. Parrot, Computational study of optimum and off-design performance of checkerboard liners, *10th AIAA/CEAS Aeroacoustics Conference* (*25th AIAA Aeroacoustics Conference*), *AIAA*-2004-3030, Manchester, UK, 2004.
[11] J. Yu, E. Nesbitt, Quiet Technology Demonstrator 2 intake liner design and validation, *12th AIAA/CEAS Aeroacoustics Conference* (*27th AIAA Aeroacoustics Conference*), *AIAA*-2006-2458, Cambridge, MA, 2006.
[12] R. Mani, US Patent 3937590: acoustic duct with peripherally segmented acoustic treatment, 1976.
[13] M.S. Howe, The attenuation of sound in a randomly lined duct, *Journal of Sound and Vibration* 87 (1) (1983) 83–103.

[14] D.L. Lansing, W.E. Zorumski, Effects of wall admittance changes on duct transmission and radiation of sound, *Journal of Sound and Vibration* 27 (1) (1973) 85–100.
[15] W.E. Zorumski, NASA TR R-419: acoustic theory of axisymmetric multisectioned ducts, Technical Report, 1974.
[16] K.J. Baumeister, Evaluation of optimized multisectioned acoustic liners, *AIAA Journal* 17 (11) (1979) 1185–1192.
[17] M.S. Tsai, Mode scatterer design for fan noise suppression in two-dimensional ducts, *Journal of Sound and Vibration* 83 (4) (1982) 501–512.
[18] J.F. Unruh, Finite length tuning for low-frequency lining design, *Journal of Sound and Vibration* 45 (1) (1976) 5–14.
[19] J.M. Tyler, T.G. Sofrin, Axial flow compressor noise studies, *Transactions of the Society of Automotive Engineers* 70 (1962) 309–332.
[20] T.R. Law, Multi-segmented Liner Optimisation for Mixed Exhaust Aeroengines, PhD Thesis, University of Cambridge, 2008.
[21] L. Lafronza, A. McAlpine, A.J. Keane, R.J. Astley, Response surface method optimization of uniform and axially segmented duct acoustics liners, *Journal of Aircraft* 43 (1) (2006) 1089–1102.
[22] M.K. Myers, On the acoustic boundary condition in the presence of flow, *Journal of Sound and Vibration* 71 (3) (1980) 429–434.
[23] W. Eversman, Theoretical models for duct acoustic propagation and radiation, *Aeroacoustics of Flight Vehicles: Theory and Practice, Vol. 2: Noise Control, NASA RP*-1258, 1991, pp. 101–163.
[24] C.L. Morfey, Sound transmission and generation in ducts with flow, *Journal of Sound and Vibration* 14 (1) (1971) 37–55.
[25] R.E. Motsinger, R.E. Kraft, *Aeroacoustics of Flight Vehicles: Theory and Practice, Vol. 2: Noise Control*, 1991, pp. 165–206.
[26] A.W. Guess, Calculation of perforated plate liner parameters from specified acoustic resistance and reactance, *Journal of Sound and Vibration* 40 (1) (1975) 119–137.
[27] A. Cummings, High frequency ray acoustics models for duct silencers, *Journal of Sound and Vibration* 221 (4) (1999) 681–708.
[28] S.H. Ko, Sound attenuation in acoustically lined circular ducts in the presence of uniform flow and shear flow, *Journal of Sound and Vibration* 22 (2) (1972) 193–210.
[29] ESDU, Item 00012: the acoustic attenuation of absorbent linings in cylindrical flow ducts, 2000.